AGU PUBLICATIONS

JGR

Journal of Geophysical Research: Oceans

RESEARCH ARTICLE

10.1002/2016JC011744

The role of bubbles during air-sea gas exchange

Steven Emerson[1] and Seth Bushinsky[2]

[1]School of Oceanography, University of Washington, Seattle, Washington, USA, [2]Now at Atmospheric and Oceanic Sciences Program, Princeton University, Princeton, New Jersey, USA

Key Points:
- Surface ocean oxygen supersaturation is controlled by gas exchange and net biological production
- Different bubble models predict a wide range of gas supersaturation as a function of wind speed
- Measurements of N_2, Ar, Ne and Kr are used to evaluate the accuracy of bubble models

Correspondence to:
S. Emerson,
emerson@u.washington.edu

Citation:
Emerson, S., and S. Bushinsky (2016), The role of bubbles during air-sea gas exchange, *J. Geophys. Res. Oceans*, *121*, 4360–4376, doi:10.1002/2016JC011744.

Received 20 FEB 2016
Accepted 23 MAY 2016
Accepted article online 27 MAY 2016
Published online 25 JUN 2016

Abstract The potential for using the air-sea exchange rate of oxygen as a tracer for net community biological production in the ocean is greatly enhanced by recent accuracy improvements for in situ measurements of oxygen on unmanned platforms. A limiting factor for determining the exchange process is evaluating the air-sea flux contributed by bubble processes produced by breaking waves, particularly during winter months under high winds. Highly accurate measurements of noble gases (Ne, Ar & Kr) and nitrogen, N_2, in seawater are tracers of the importance of bubble process in the surface mixed layer. We use measured distributions of these gases in the ventilated thermocline of the North Pacific and an annual time series of N_2 in the surface ocean of the NE Subarctic Pacific to evaluate four different air-water exchange models chosen to represent the range of model interpretation of bubble processes. We find that models must have an explicit bubble mechanism to reproduce concentrations of insoluble atmospheric gases, but there are periods when they all depart from observations. The recent model of Liang et al. (2013) stems from a highly resolved model of bubble plumes and categorizes bubble mechanisms into those that are small enough to collapse and larger ones that exchange gases before they resurface, both of which are necessary to explain the data.

1. Introduction

Net biological oxygen production in the surface ocean (to the depth of the winter mixed layer), if integrated over an entire year, is, via stoichiometry, equal to the annual net community production of carbon (ANCP). At steady state this value must equal organic carbon export (sometimes called the biological carbon pump, see *Emerson* [2014]). The magnitude and geographic distribution of this value is of interest to oceanographers because it has an important effect on atmospheric pCO_2 levels and the distribution of oxygen and other metabolites in the thermocline and deep sea.

The net biological oxygen production can be determined from a time series of oxygen measurements if the physical processes affecting the oxygen supersaturation can be evaluated in an upper ocean model. The leading physical process controlling oxygen concentrations in the ocean mixed layer is air-sea gas exchange, and the role of bubbles caused by breaking waves is a first order process when winds are strong. Another inert gas (e.g., Ar or N_2) is often measured to sort out the physical and biological processes that affect O_2 supersaturation when using oxygen measurements in the surface ocean to calculate biological rates of net community production [e.g., *Spitzer and Jenkins*, 1989, *Emerson et al.*, 2008]. Since it is currently not possible to measure either Ar or N_2 on profiling floats and gliders, and frequently not practical on ships of opportunity (Voluntary Observing Ships, VOS), an accurate theoretical estimate of the degree of supersaturation caused by bubble processes is necessary when using in situ measurements of oxygen to determine biological fluxes.

Our purpose here is to demonstrate how available inert gas data constrain the validity of models used to calculate bubble-produced gas supersaturation. We interpret highly accurate measurements of N_2/Ar, Ne, Ar, and Kr in the ventilated thermocline of the North Pacific Ocean and year-long, surface-ocean measurements of N_2 on a surface mooring at Ocean Station Papa (OSP, 50° N, 145° W). Four different published models of air-sea gas transfer as a function of wind speed are employed in two separate upper-ocean models to calculate the expected degree of inert gas supersaturation. By comparing model predictions with data, we infer the accuracy of the available models for calculating the role of bubbles in creating surface oxygen supersaturation.

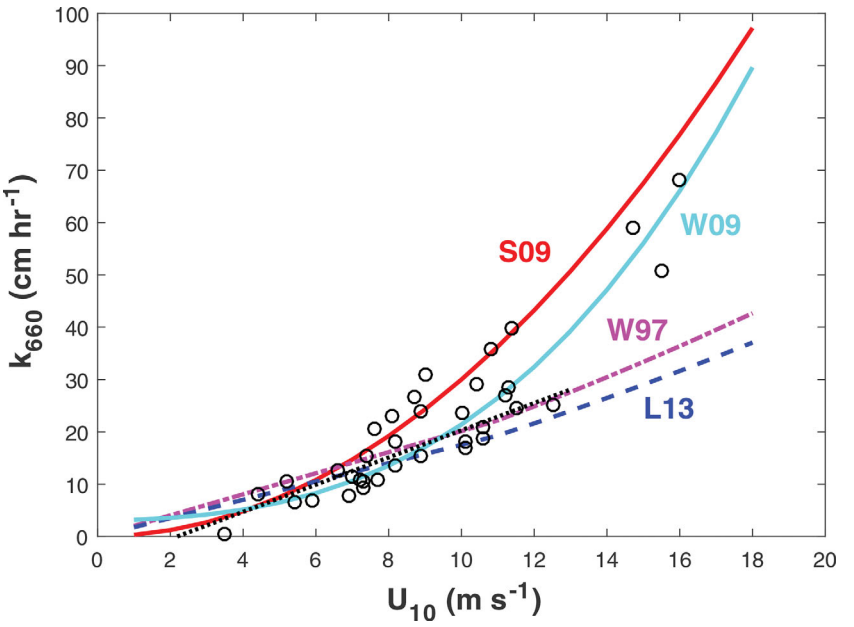

Figure 1. The air-water interface mass transfer coefficient, k_s, at a Schmidt number of 660 (CO_2 at 20°C in seawater) as a function of wind speed at 10 meters height. Lines represent the relationships from different models of gas exchange [*Stanley et al*., 2009, hereinafter S09; *Wanninkhof et al*., 2009, hereinafter W09; *Woolf*, 1997, hereinafter W97; *Liang et al*., 2013; hereinafter L13]. The unlabeled, black line is a suggested value for k_s based on atmospheric eddy correlation fluxes of DMS from the ocean [*Goddijn-Murphy et al*., 2016] Circles (o) are data from purposeful tracer release experiments excluding three points from the SoFex experiment, which have very large error estimates [*Ho et al*., 2011].

2. Background

The transfer of gases into the surface ocean by bubbles produced during wave breaking has long been recognized as an important process causing gas supersaturation [*Kanwisher*, 1963; *Fuchs et al*., 1987; *Merlivat and Memery*, 1983; *Woolf and Thorpe*, 1991; *Keeling*, 1993]. This is especially true for the more insoluble gases that make up most of the atmosphere (N_2, O_2, and all noble gases) because forced injection of atmospheric gas into surface water by subduction of bubbles causes a greater elevation of the dissolved concentration for these gases. Noble gas and N_2 measurements in the upper ocean have been used to constrain bubble models before [*Spitzer and Jenkins*, 1989; *Hamme and Emerson*, 2006, *Steiner et al*., 2007; *Stanley et al*., 2009, *Vagle et al*., 2010], but there is not a consensus about which models are most accurate [*Nicholson et al*., 2011, *Liang et al*., 2013]. We now have a highly-accurate, world-wide data set for the N_2/Ar ratio [*Hamme and Emerson*, 2013], which is very sensitive to bubble processes but not sea-surface temperature changes. We use these data combined with deep-ocean noble-gas measurements [*Hamme and Severinghaus*, 2007] and a time series of surface-ocean nitrogen gas concentrations at Ocean Station Papa (OSP) to determine the accuracy of present models.

There are many different model approaches to evaluating the importance of bubbles in air-sea gas exchange. We choose four different models in use presently and which represent a wide range of possible behavior ascribed to bubbles. A description of these models, along with the equations used, and how they are related to each other is presented in the Appendix A. We introduce them briefly here. The model of *Wanninkhof et al*. [2009, hereinafter W09; equation (A2)] is used here as an end member case because it does not explicitly include bubble flux terms. However, this model does have a cubic wind-speed dependence in the high range, which is similar to the wind speed correlation to whitecaps that are an indication of bubble formation. The mass transfer coefficient variation with wind speed in W09 is tuned to the ocean inventory of bomb-produced ^{14}C and purposeful tracer release experiments (Figure 1).

One of the traditional gas exchange bubble models (*Woolf and Thorpe* [1991] and later *Woolf* [1997, hereinafter W97]) derived air-sea fluxes from a physical model of bubble plume dynamics. There are three unknown parameters in this set of equations (Appendix A, equations (A4)–(A9)). First, the transfer coefficient describing air-sea interface exchange, k_s, as a function of wind speed was adopted from wind tunnel

experiments of *Jahne et al*. [1987]. This trend is very similar to the first two linear portions of the well-known gas transfer coefficient-wind speed dependence described by *Liss and Merlivat* [1986], the NOAA-COARE formulation for gas exchange [*Fairall et al*., 2003], and the results of DMS atmospheric eddy correlation measurements over the oceans [*Goddijn-Murphy et al*., 2016] (see Figure 1). Bubble processes in this model are parameterized using a bubble mass transfer coefficient, k_b, and a bubble–induced fractional superstation, Δ_e. The latter value describes the steady-state degree of supersaturation, ([C] - [C^s](1+ Δ_e), mol m^{-3}) required to drive a gas flux to the atmosphere by air-water surface exchange, that exactly balances the influx by bubbles. Values of the wind speed necessary to create a Δ_e of 1% are given by Woolf and Thorpe [1991] for O_2, N_2 and CO_2.

Gas transfer models that evolved from the desire to interpret observed supersaturation of noble gases, originally helium, envisioned two categories of bubble fluxes: one flux from small bubbles that are forced to great enough depths to collapse, F_c, and another flux from larger bubbles, F_p, that enter the ocean, exchange gases, and then resurface to the atmosphere [*Fuchs et al*., 1987, *Jenkins*, 1988, equations (A11)–(A13)]. The unknowns in these models are the surface air-sea mass transfer coefficient, k_s, a mass transfer coefficient for each of the two bubble processes, k_c and k_p, respectively, and the difference between the partial pressure in the surface waters and that inside the larger bubbles, ΔP. The primary cause of the supersaturation inside the bubbles is hydrostatic pressure as they are transported below the air-water interface.

Stanley et al. [2009, hereinafter S09] used the collapsing-and-exchanging bubble mechanisms in a one-dimensional, upper-ocean mixing model to calculate the gas exchange mass transfer coefficients from annual measurements of noble gases (He, Ne, Ar, Kr, Xe) in the surface waters of the Sargasso Sea. In her version of the model (equations (A14)–(A18)), ΔP was calculated from a function that relates the depth of penetration of bubble plumes to wind speed (equation (A15)). Values for the gas exchange mass transfer coefficients, k_s, k_c and k_p and their relationship to wind speed were determined by simulating concentrations of the noble gases in the upper ocean model.

The most recent of the bubble models [*Liang et al*., 2013, hereinafter L13] is a direct calculation of bubble-induced gas fluxes from a large eddy simulation model coupled with a bubble population model. Gas transfer across the bubble surface followed the same mechanisms used by *Fuchs et al*. [1987] and S09. Results were compared with observations of argon supersaturation in the ocean. The model of L13 adopts the air-sea mass transfer coefficient, k_s, from the NOAA-COARE model of gas exchange [*Fairall et al*., 2003, 2011; *Hare et al*., 2004; equation (A19)] and then solves for the wind speed dependency of the two bubble mass transfer coefficients, k_c and k_p, and the large bubble supersaturation, ΔP.

The wind-speed dependence of the air-sea surface gas transfer coefficients in these four models are dramatically different (Figure 1). The trends for those of S09 and W09 are quadratic to cubic with respect to wind speed and follow the observations from tracer-release experiments. The k_s values in Figure 1 for both W97 and L13 are nearly linear with respect wind speed and are much less than the results from tracer-release experiments above wind speeds of about 10 m s^{-1}. At higher winds the latter models require bubble processes comparable in magnitude to the surface exchange to explain the observations.

3. Results and Discussion

3.1. Noble Gas and N_2/Ar Data Used to Constrain Bubble Processes

Data used to test the bubble models are presented here as the degree of supersaturation with respect to atmospheric equilibrium in percent: $\Delta C\ (\%) = \{([C]-[C^s])/[C^s]\}100$, where [C] is the concentration of the gas (mol kg^{-1}) and [C^s] is the concentration at saturation equilibrium with the atmosphere at the measured temperature, salinity and pressure. Saturation equilibrium values as a function of temperature and salinity are those of *Hamme and Emerson* [2004] for N_2, Ar and Ne and the values of *Weiss and Kyser* [1978] for Kr (See Figure 2). A pressure of one atmosphere is assumed by default for all measurements in the ocean interior. The data used here are of two types: the first are noble gas concentrations and N_2/Ar ratios measured in the North Pacific subtropical ocean in the mode waters that subduct into the thermocline from surface outcrops between the subarctic and subtropical gyres [e.g., *Suga et al*., 2004]. The second are the N_2 gas concentrations measured remotely every 3 h at about two meters depth on a surface mooring at Ocean Station Papa (OSP) in the subarctic ocean.

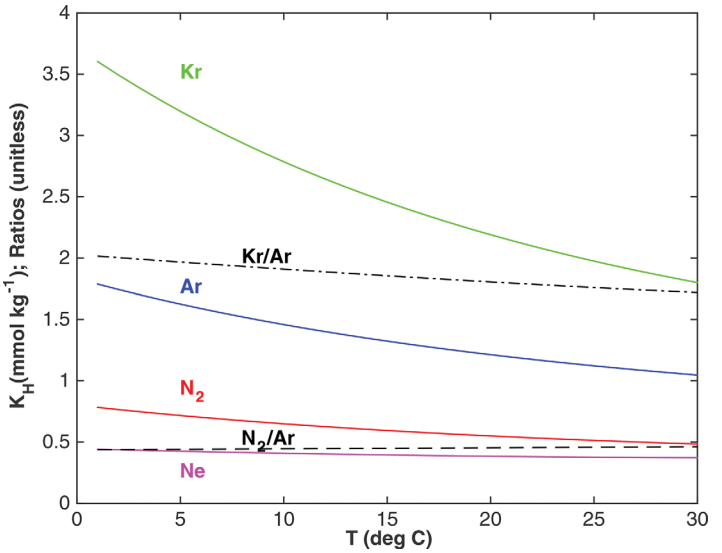

Figure 2. The Henry's Law Solubility coefficient at one atmosphere (mmol kg^{-1}) as a function of temperature for Ne, Ar, Kr and N_2. The ratios N_2/Ar and Kr/Ar are also presented to show how the ratio mostly eliminates the temperature dependence. The nonlinearity of solubility with temperature causes supersaturation when saturated waters of different temperatures mix.

3.1.1. North Pacific Thermocline

Waters in the upper thermocline of the North Pacific are formed at the ocean surface in wintertime. The location and characteristics of the "Mode Water" formation in winter are described by *Suga et al.*, [2004]. Wintertime characteristics of this region taken from this reference and from reanalysis by the NOAA-ESRL global circulation model are presented in Table 1.

The noble gas and N_2/Ar data in the upper thermocline of the North Pacific (Figure 3) were "preformed" at the ocean surface in the Mode Water formation region. These data are compiled here from measurements published previously and available on the web. N_2/Ar, Ar and Ne data are averages of 6–12 depth profiles to 1000 m over a period of 1 year at the Hawaii Ocean Time series (HOT) (see *Hamme and Emerson* [2006], and the data compilation on Hamme's website, www.uvic.ca/~rhamme/). Krypton results are from a single profile published in *Hamme and Severinghaus* [2007] from the same location. We are interested in data from pressures deep enough to be unaffected by local heating processes ($>$ 200 m) and from within the density range of waters that originate in the winter at the surface in the North Pacific ($\sigma_\theta < 26.6 - 26.7$). The number of sample duplicates from the web database within this density interval are 5 for Ne and 11 for N_2/Ar and Ar (column two of Table 2). The ratios of the standard deviations to the means of these measurements are $\pm$ 0.2%, $\pm$ 0.1%, and $\pm$ 0.3%, respectively. The estimated precision of duplicate Kr measurements on a single profile by *Hamme and Severinghaus* [2007] was $\pm$ 0.2%.

Mechanisms that control inert gas supersaturation, ΔC, in the ocean interior are: (1) temperature change and air-sea gas transfer with the atmosphere at the surface ocean outcrop, (2) the atmospheric pressure at the location and time of the outcrop, (3) mixing of waters across temperature gradients in the interior, which can create supersaturation, and (4) nitrogen gas has a biological component in some ocean interior locations due to denitrification. We discuss these processes in more detail below and argue that we can correct the data for processes (2) through (4).

Subduction of surface waters to the ocean interior occurs in the wintertime when cooling increases density. Temperature decrease creates gas undersaturation because cold water can hold more gas at thermodynamic equilibrium and gas exchange is relatively slow. Bubble fluxes caused by breaking waves at high wind speeds have the opposite effect of creating gas supersaturation. These two processes compete to drive the saturation state of the inert gases away from equilibrium while surface air-sea exchange pulls the concentrations back toward atmospheric saturation. Fortunately, the saturation temperature dependence and solubility of the inert gases varies enough (Figure 2) to distinguish the importance of these different processes [see *Hamme and Emerson*, 2006; *Hamme and Severinghaus*, 2007].

Table 1. Characteristics of the Winter-Time (October–February) Outcrop of the Central Mode Water

Ocean Characteristics [*Suga et al.*, 2004]:
Outcrop region 36–42° N; 145°E – 170°W
Density range, σ_θ = 26.0–26.6.
Mixed layer depth = 150 – 200 m
Atmosphere (NOAA-ESRL Reanalysis):
Surface ocean temperature change between Oct and Feb = 15.5–10.0°C (−0.4°C d^{-1})
Mean daily wind speed (Oct. – Feb.) = 12.3 m s^{-1}
Sea level pressure = 1009 mbar (0.4% below one atmosphere)

Once the subducting waters escape the ocean surface, gases are isolated from physical processes that change their concentration. However, diapycnal mixing creates supersaturation if the gas saturation

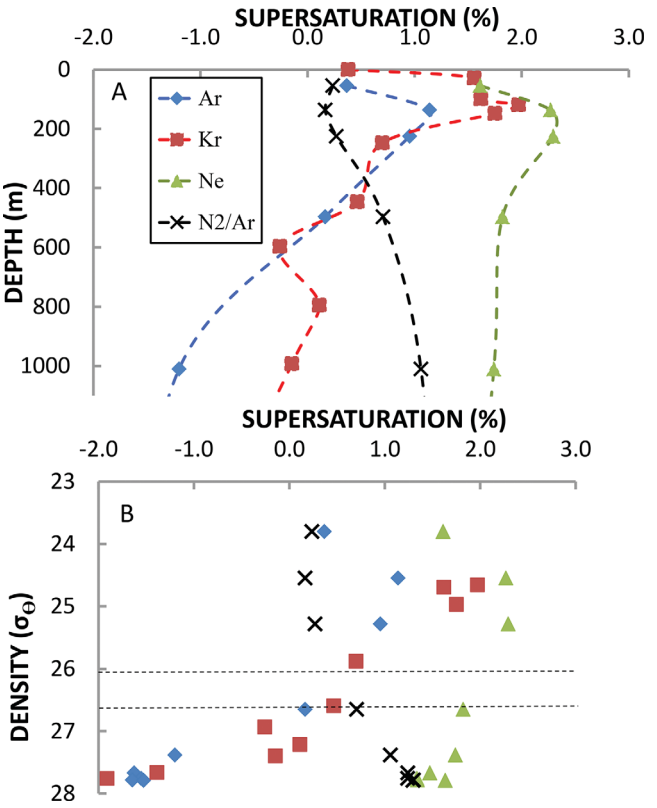

Figure 3. Profiles of Ar, Kr, Ne, and N_2/Ar supersaturation in percent, $\Delta C = \{([C] - [C^{sat}])/[C^{sat}]\} \times 100$, at the Hawaii Ocean Time Series. N_2/Ar, Ne, and Ar data are mean values from an annual time series of data and each depth represents 6–12 duplicate measurements [*Hamme and Emerson*, 2006]. Krypton data are from a single profile [*Hamme and Severinghaus*, 2007]. All the data can be found in tabular form on Roberta Hamme's website (www.uvic.ca/~rhamme/).

concentrations are nonlinear with respect to temperature because mixing end members at saturation will create a mixture that is supersaturated (see Figure 2). The effect of diapycnal mixing on the argon supersaturation in the ocean thermocline in the North Pacific was determined by *Emerson et al.* [2012] by measuring Ar concentrations on north-south transects from the mode water outcrop into the subtropical gyre. They found supersaturation increases that averaged 0.5 ± 0.2% over the circulation distance between ~ 40° N and ~20° N near the Hawaii Ocean Time series (HOT) site. *Ito and Deutsch* [2006] derived an analytical expression that related the supersaturation concentration, $\delta C = [C] - [C^s]$, induced by diapycnal mixing on a surface of constant density to the product of: the second derivative of the equilibrium saturation value as a function of temperature, the diapycnal diffusion coefficient, K_z, and the square of the change in temperature with respect to depth.

$$\partial C = K_z \left(\partial T / \partial z\right)^2 \partial^2[C^s] / \partial T^2 \quad (1)$$

The measured argon supersaturation of 0.5% in this model required a diapycnal diffusion coefficient of about 1×10^{-5} m^2 s^{-1}. The supersaturation ratio of gas C, δC, compared to that for argon, δAr, is equal to the ratios of the curvature of the solubility temperature dependence:

$$\frac{\delta C}{\delta Ar} = \frac{\partial^2[C^s]/\partial T^2}{\partial^2[Ar^s]/\partial T^2} \quad (2)$$

Adopting a mixing-induced saturation anomaly for Ar, of 0.5%, results in mixing-induced supersaturation for ΔNe and Δ Kr of +0.2%, and +0.7%, respectively. For the ratio Δ(N_2/Ar) the mixing increase is only 0.1% because the solubility temperature dependences are similar for these two gases (Figure 2). These corrections are applied to the data in the third column of Table 2.

Table 2. Measured Gas Supersaturation and Supersaturation Ratios (in %) in the Density Range, σ_θ = 26.0 – 26.7 Taken From the Data Base Described in the Text[a]

Gas (Gas Ratio) (%)	Data	After Diff. Corr.	After Pressure Corr.
ΔNe	+1.7 ± 0.2 (n=5)	+1.6	+2.0
ΔAr	+0.1 ± 0.3 (n=11)	−0.4	+0.0
ΔKr	+0.4 ± 0.2 (n=2)	−0.2	+0.2
ΔN_2/Ar	+0.6 ± 0.1 (n=11)	+0.7[b]	+0.7
ΔKr/Ar	+0.2 ± 0.3 (n=2)	0.0	0.0

[a]Data in column 3 have been corrected for diapycnal diffusion (−0.1, −0.5, and −0.6% for ΔNe, ΔAr, and ΔKr and −0.1% for Δ(N_2/Ar)* and Δ(Kr/Ar), see text). Data in column 4 have been corrected for both diapycnal diffusion and the atmospheric pressure at the location and time of the surface outcrop (+0.4% for all gases and no correction for gas ratios).

[b]The biological correction for Δ(N_2/Ar) is +0.05% and the diffusion correction is −0.1% so they are assumed to cancel (see text).

Nitrogen fixation in the surface ocean has the potential to increase the N_2 concentration before it leaves the surface, but one can show that even the highest estimates of N_2 fixation have an unmeasurable effect on N_2 concentrations in surface ocean waters that are continuously exchanging with the atmosphere. There are; however, measurable increases in ΔN_2 in

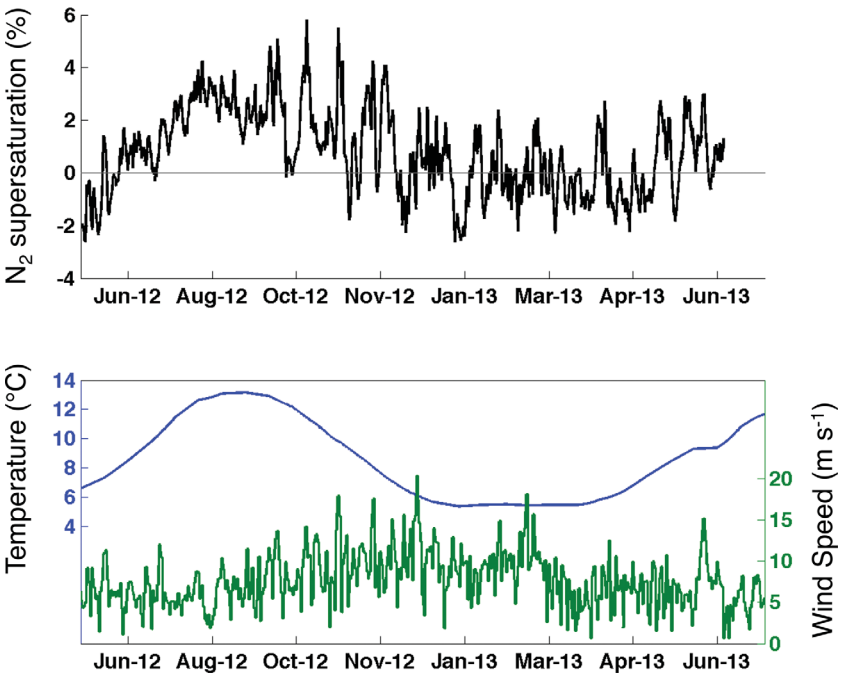

Figure 4. The degree of N_2 supersaturation, surface temperature, and wind speed from in situ measurements on a surface mooring at Ocean Station Papa (OSP, 145°W, 50° N) for the year June 2012 to June 2013. N_2 supersaturation (Top) and temperature (Bottom) are at 2 meters depth in surface waters. Wind speed (Bottom) is at 10 meters height in the atmosphere. Gas data are unpublished and available on request from the authors; wind data can be down loaded from the NOAA-PMEL mooring website.

the ocean interior caused by denitrification in locations where oxygen concentrations are low [*Chang et al.*, 2010]. We correct the $\Delta(N_2/Ar)$ ratios in Figure 3 for the N_2 concentrations added by denitrification using values of N* determined from the same water. N* is defined as the deficiency of NO_3^- relative to that expected from the concentration of total dissolved phosphorus (DIP) times the N/P Redfield ratio [*Gruber and Sarmiento*, 1997].

$$N^* = [NO_3^-] - 16[DIP]\ (\text{mol m}^{-3}) \tag{3}$$

During denitrification the concentration of N_2 should increase by one half the NO_3^- decrease, so the $\Delta(N_2/Ar)$ ratio corrected for this effect is defined as:

$$\Delta(N_2^*/Ar) = \Delta(N_2/Ar) - 0.5\{N^*/[Ar])_{meas}/(N_2/Ar)^{sat}\} \times 100 \tag{4}$$

The conservative tracer $\Delta(N_2^*/Ar)$ was determined from the data used here by calculating N* from the nutrient data of the HOT program (http://www.hahana.hawaii.edu). The correction is very small, $\sim +0.05\%$ and of the same magnitude but of the opposite sign to that estimated for the mixing correction for this ratio, so we elected to make no change for these effects (Table 2).

The final correction to the data is due to atmospheric pressure during the winter months at about 40° N in the Northwest Pacific where the mode waters form. Sea level pressure in the wintertime at this location from reanalysis models was 1009 mbar, which is 0.4% below one atmosphere (Table 1). The data (Figure 3) assume one atmosphere for the gas supersaturation calculation. If the true wintertime value is below one atmosphere, environmentally-induced supersaturations are 0.4% greater than indicated. Supersaturations are corrected for this effect (column 4 in Table 2) except for gas ratios where differences in the ambient atmospheric pressure cancels.

3.1.2. NE Pacific Surface Ocean N_2 Data

Surface water N_2 measurements determined every 3 h during the year 2012 at Ocean Station Papa (OSP, 145° W, 50° N; Figure 4) derive from a combination of in situ oxygen and gas tension device (GTD) [see *McNeil et al.*, 1995] measurements on a surface mooring. The GTD determines highly accurate total gas pressure using a Paroscientific pressure sensor and oxygen is measured using an Aanderaa optode calibrated by Winkler oxygen titrations. Assuming argon concentrations are near the value expected for saturation equilibrium with the atmosphere yields N_2 gas pressures that are accurate to a few tenths of one percent. (See

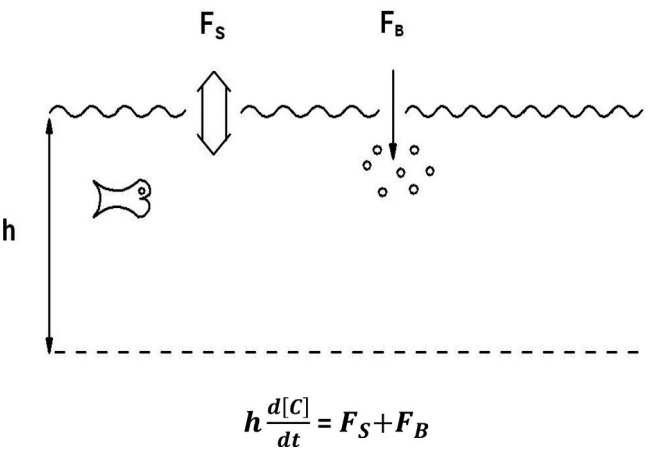

Figure 5. A schematic diagram depicting the surface-ocean model used to predict the degree of supersaturation of inert atmospheric gases in the mode water formation area in winter. [C] is the gas concentration (mol m^{-3}), h is the winter time mixed layer depth (m), and F_S and F_B fluxes are due to exchange at the air-water interface and bubbles, respectively.

Emerson et al. [2002], for a description of the methods used to determine N_2 from O_2 and GTD measurements.) The measurements (Figure 4) indicate supersaturation in summer caused mainly by warming, and then fluctuations around $\Delta N_2 = 0$ in winter caused by the combination of cooling and bubble processes. The ΔN_2 data have a spikey nature primarily because short-term changes in atmospheric pressure due to local storms create an immediate response for atmospheric pN_2 but a much slower response of the pN_2 in the surface ocean.

3.2. Upper Ocean Models

3.2.1. Surface Ocean and Ventilated Thermocline

The model used to interpret the inert gas data from the North Pacific thermocline is a simple quasi-steady-state solution for gas concentrations in an idealized mixed layer of constant depth, h (Figure 5), which is horizontally homogeneous and has no exchange with water below the mixed layer. Wintertime temperature in the model decreases linearly with time and gases exchange with the atmosphere via both surface air-water exchange, F_s, and bubble processes, F_b. This is clearly a crude representation of surface ocean processes before the water ventilates into the thermocline, but we believe it captures the main processes controlling inert gas supersaturation: surface water cooling and atmosphere-ocean gas exchange by both air-water interface diffusion and bubble processes.

The change in concentration of gas C in the ocean mixed layer is described by:

$$h\frac{\partial [C]}{\partial t} = F_s + F_b \ \left(\text{mol m}^{-2}\text{d}^{-1}\right) \tag{5}$$

where F_s and F_b are defined for the four different air-sea exchange models described in the Appendix A. The gas saturation concentration, $[C^s]$, is:

$$[C^s] = [C^{s,0}] + mt \ \left(\text{mol m}^{-3}\right) \tag{6}$$

where, $[C^{s,o}]$ is the initial saturation concentration at t=0 and the saturation concentration temperature, T, dependence with time, t, is described by

$$m = \frac{\Delta [C^s]}{\Delta \text{T}} \frac{\Delta \text{T}}{\Delta \text{t}} \ \left(\text{mol m}^{-3}\right) \tag{7}$$

The time dependent solution to this ordinary differential equation is (see the Appendix A for a description of the terms and their units):

$$[C](t) = \left(m + \frac{m\Delta Pk_p}{ha}\right)t - \left(\frac{m}{a}\right)(1-e^{-at}) - \frac{m\Delta Pk_p}{ha^2}(1-e^{-at}) + \left(\frac{A}{a}\right)(1-e^{-at}) + C^0 e^{-at} \tag{8}$$

with $A = a[C^{s,0}] + \frac{\Delta Pk_p}{h}[C^{s,0}] + \frac{k_c}{h}X^c$ and $a = \frac{k_s + k_p}{h}$

At quasi steady state, when the degree of supersaturation becomes invariant in time because the rate of cooling, and hence production of undersaturation, is balanced by the air-sea exchange processes, the above equation becomes:

$$\frac{[C]-[C^s]}{[C^s]} = -h\frac{\Delta [C^s]}{\Delta T}\frac{\Delta T}{\Delta t}\frac{1}{[C^s]}\left\{\frac{1}{k_s+k_p} + \frac{\Delta Pk_p}{(k_s+k_p)^2}\right\} + \frac{\Delta Pk_p}{k_s+k_p} + \frac{k_c}{k_s+k_p}\frac{X^c}{[C^s]} \tag{9}$$

This equation is applied to the data in two ways. First, the degree of supersaturation (the left side of equation (9)) is calculated as a function of wind speed for the mass transfer coefficients k_s, k_c, and k_p given in four different models of gas exchange described in the Appendix A. In this case we assumed that the rate of cooling, $\Delta T/\Delta t$, is known from reanalysis (Table 1). The second approach involves simultaneous solution of three versions of equation (9) for the data: $\Delta(N_2/Ar)$, ΔNe and $\Delta(Kr/Ar)$ to obtain values for $\Delta T/\Delta t$, k_p and k_s. We use $\Delta T/\Delta t$ as an unknown so we can compare the result to what we expect from the reanalysis estimates and thus verify that the solutions are accurate. The different approaches give similar results, and are both used in the next section. Calculation of the degree of supersaturation as a function of wind speed (U_{10}) is compared with data to determine the bubble model accuracy, and the simultaneous solution was used for the error analysis.

3.2.2. Surface Ocean N_2 Data at OSP

A separate upper ocean model is used to compare the nitrogen supersaturation measurements in surface waters at OSP with values predicted from the four separate gas exchange formulations. The model used here is described in *Bushinsky and Emerson* [2015] and will be reviewed only briefly. This upper ocean model compartmentalizes the surface 150 meters of the ocean into a variable-height mixed layer above a series of 1.5 m layers. Changes in the concentration of N_2 in all layers are stepped forward in time for a period of 1 year considering independently derived advective fluxes, mixed layer entrainment, eddy diffusion, and air-sea gas transfer. Advection velocities are calculated from reanalysis currents and horizontal gradients from climatological estimates of N_2 supersaturation. Eddy diffusion coefficients below the mixed layer are those described from heat and salt balances by *Cronin et al*. [2015]. The model incorporates values of T, S and mixed-layer depth measured by profiling floats in the OSP area. In this way the N_2 saturation value and hence ΔN_2 in the mixed layer are not dependent on the ability of the model to reproduce measurements of T and S. With this model we give up prognostic ability to accurately incorporate the factors that determine gas supersaturation. The most important terms in the N_2 mass balance are the time rate of change, and air-sea fluxes. Entrainment is significant when the mixed layer deepens rapidly, and vertical diffusion is influential in the winter when the mixed layer is deepest [see *Bushinsky and Emerson*, 2015]

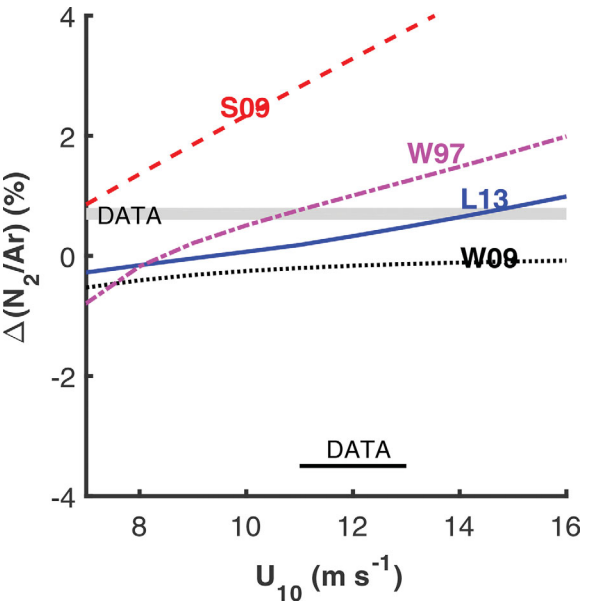

Figure 6. Comparison of model results with N_2/Ar supersaturation data in the Mode Water density interval of the North Pacific. Lines represent the quazi steady-state model solution (equation (9)) as a function of wind speed for different gas exchange models labeled by the symbols described in the caption for Figure 1. The gray field labeled "Data" represents the data in the mode waters between $\sigma_\theta = 26.0 - 26.7$ presented in Figure 3 and Table 2 and the line labeled "Data" is the mean and standard deviation of the winter time wind speed in this region from NOAA-ESRL reanalysis (Table 1). Each model line has a confidence interval of ± 0.2% on the ordinate as discussed in the text and indicated in Table 3.

3.3. Model-Data Comparisons

3.3.1. North Pacific Thermocline

Predicted inert gas supersaturations in the ocean thermocline as a function of wind speed (Figures 6–9) vary dramatically depending on the different gas exchange models used. We show later that the error in predicting the supersaturation given our best guess uncertainties for the input terms is on the order of ± 0.2–0.5% supersaturation for the gas ratios and ΔNe and more like ± 1.0–1.5% supersaturation for ΔAr and ΔKr. The first conclusion from this analysis is that the gas exchange model without bubble processes cannot explain the inert gas data. The degree of supersaturation predicted from the W09 model is less than the data in every case (Figures 6–9), presumably because there is no explicit mechanism for inserting atmospheric gases into the upper ocean when cooling tends to produce undersaturation. For more soluble gases (i.e., CO_2) a mass transfer coefficient-wind speed dependence that includes a cubic term at high winds may approximate reality, but not for the more insoluble atmospheric gases.

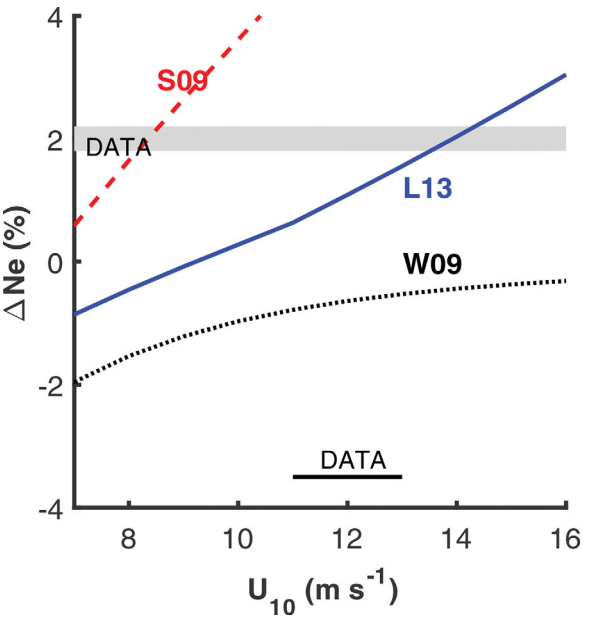

Figure 7. Comparison of model results as a function of wind speed with data for Ne supersaturation. The lines and field are as described in the caption for Figure 6. Each model line has a confidence interval of ± 0.6% on the ordinate as discussed in the text and indicated in Table 3. There is no model line for W97 because the Δ_e value for Ne was not determined for this model.

The second major observation is that the model of S09 predicts much higher supersaturation for the most insoluble gases—ΔN_2/Ar and ΔNe (Figures 6 and 7) than the observations. The S09 model predicts a quadratic function for interface air-sea exchange similar to that of *Wanninkhof* [1992] and *Nightingale et al.* [2000] and a strong forcing for bubbles that collapse (k_c) with very little contribution due to larger bubbles (k_p). This dominance of small bubbles was not found in other similar studies [*Hamme and Emerson*, 2006, *Liang et al.*, 2013] and appears to be unable to explain the inert gas data here as well. The model of S09 predicts the observed ΔAr supersaturation at a wind speeds that are ~2 m s^{-1} slower than the predictions by the L13 and W97 models. This difference is not great enough to distinguish the models given the error associated with the model and data results (see later).

Both of the models that predict gas transfer from simulated bubble plumes [*Woolf*, 1997, hereinafter W97] and *Liang et al.* [2013, hereinafter L13] are able to reproduce the ΔN_2/Ar, ΔNe and ΔAr data (Figures 6–8). These two models also suggest an important role for larger bubbles that exchange gases (k_p) because large bubble processes are necessary in these models to interpret data at wind speeds greater than 10 m s^{-1} (Figure 1).

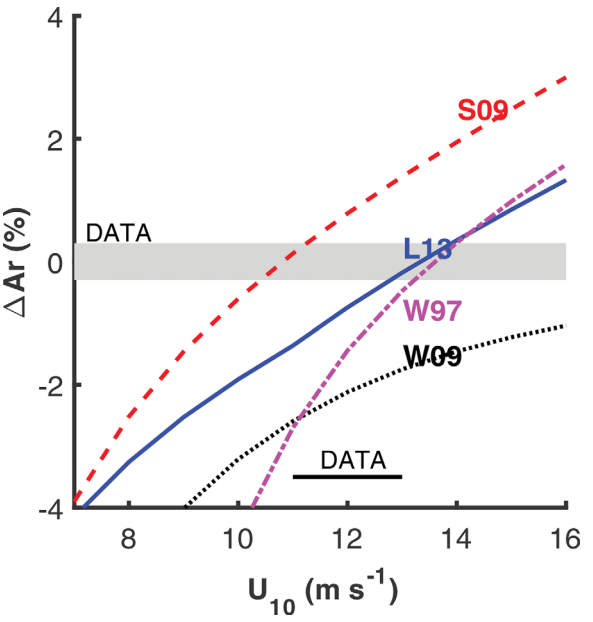

Figure 8. Comparison of model results as a function of wind speed with data for Ar supersaturation. The lines and field are as described in the caption for Figure 6. Each model line has a confidence interval of ± 1.0% on the ordinate as discussed in the text and indicated in Table 3. The Δ_e value for O_2 was used to derive the line for the W97 model.

Finally, the ΔKr/Ar supersaturation data (Figure 9) are not explained by any of the models. Among the tracers used here, Krypton is the least dependent on collapse of small bubbles and most dependent on larger bubbles and interface air-sea exchange. The measurements indicate supersaturations that are 1–2% greater than the model results. It is possible that some of the data-model difference may have to do with the uncertainty of the krypton solubility, which was determined almost 40 years ago [*Weiss and Kyser*, 1978]. More recent, but as yet unpublished laboratory experiments (D. Lott and W. Jenkins, Woods Hole Oceanographic Institution, personal communication, 2016), indicate Kr solubility in seawater at 10°C that is about 1% higher than previously published values. Definitive interpretation of the krypton data will require more certainty in the atmospheric equilibrium solubility.

3.3.2. Surface Ocean N_2 Data at OSP

Interpretation of nearly continuous N_2 data at Ocean Station Papa using the different

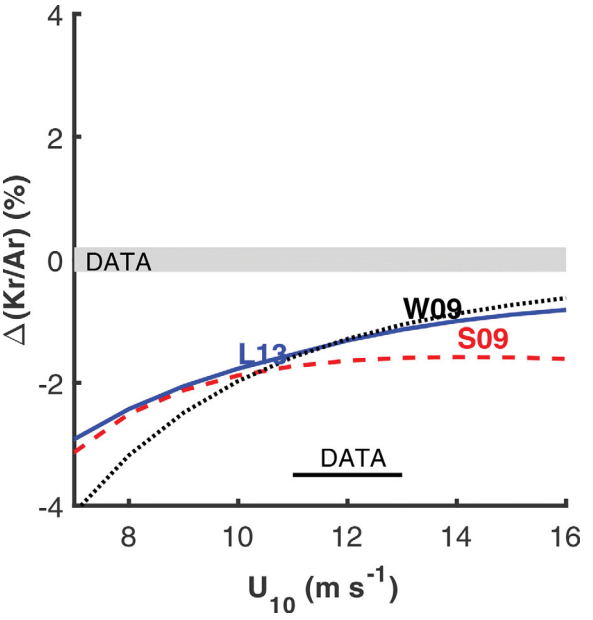

Figure 9. Comparison of model results as a function of wind speed with data for Kr/Ar supersaturation. The lines and field are as described in the caption for Figure 6. Each model line has a confidence interval of ± 0.6% on the ordinate as discussed in the text and indicated in Table 3. There is no model line for W97 because the Δ_e value for Kr was not determined for this model.

gas exchange models (Figure 10) reveals trends that are similar to those from the thermocline data: during summertime when wind speeds are relatively slow (Figure 4) all the gas exchange models, with the possible exception of S09, reproduce the data to within a few percent of supersaturation. However in winter, when wind speeds are higher and bubble processes become more important, the model with no explicit bubble processes, W09, predicts greater undersaturation than the data and S09 dramatically overpredicts supersaturation. The models of W97 and L13 do the best job of reproducing the data with L13 being the better of these two. Even these latter two models; however, predict supersaturations in late winter and early spring that are systematically higher than the data by about 2%, which probably indicates that they over predict the impact of bubbles at high wind speeds. It is certainly possible that other mechanisms not included in this simple model could be part of the reason for the data-model differences in late winter/early spring. For example, large eddies from eastern continental boundary are known to pass through OSP. Water inside the eddy would have a temperature and salinity history different from the surrounding water that might not be captured in the model even though measured temperature and

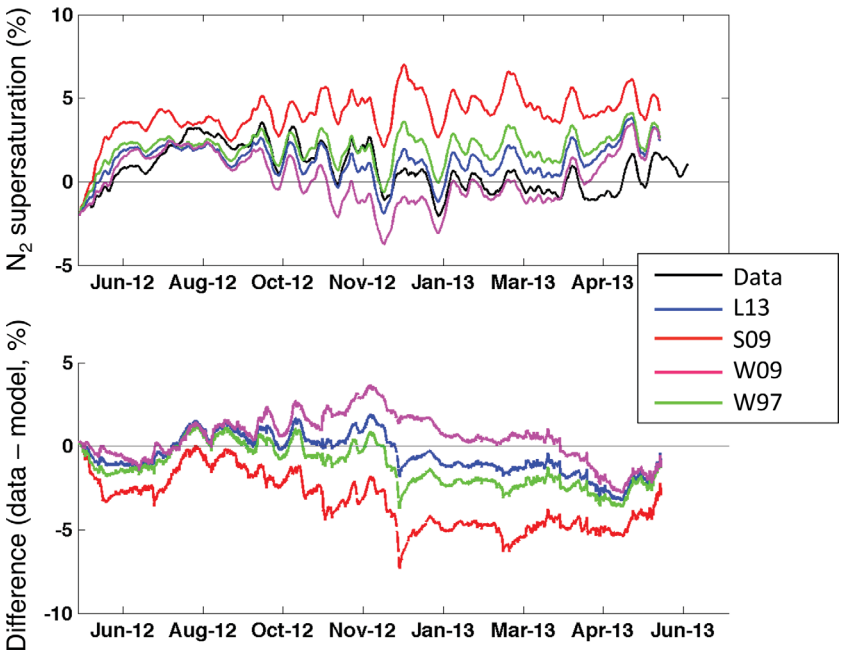

Figure 10. (top) Comparison of model results for the nitrogen supersaturation with a full year of surface ocean data at OSP. The surface model is presented in *Bushinsky and Emerson* [2015] and described briefly in the text. The black line is smoothed data (also presented in Figure 4) and the colored lines are model solutions using different gas exchange models with the symbols described in the caption to Figure 2. (bottom) The bottom figure is the difference in supersaturation between the data and each of the four models so values closest to the zero line best match the data.

Table 3. Results of Monte Carlo Error Analysis[a]

Mean and Standard Deviation of Input		Mean and Standard Deviation of Monte Carlo Error Analysis				
		ΔNe	ΔAr	ΔKr	Δ(N_2/Ar)	Δ(Kr/Ar)
h (m)	175 ± 50		−0.60 ± 0.71			
U_{10} (m s^{-1})	12.3 ± 1.2		−0.58 ± 0.52			
dT/dt (°C d^{-1})	−0.03 ± 0.01		−0.56 ± 0.50			
All		1.2 ± 0.6	−0.55 ± 1.0	−1.8 ± 1.4	0.4 ± 0.2	1.3 ± 0.6

[a]The degree of supersaturation (Δ) was calculated using equation (9) and the input values in columns 1&2. Input parameters (mixed layer depth, h; wind speed, U_{10}; and temperature change with time, dT/dt) were varied randomly around the mean using the standard deviations given. Solutions are presented for the random error of each input and for all together. The latter is on the last row. (see text).

salinity are used to determine the N_2 saturation equilibrium value. Resolving the sources of these uncertainties and improving the prediction of bubble processes in even the best preforming models will require many more data-model comparisons.

3.4. Error Analysis

Perhaps the most rigorous error analysis of the calculations here is interpretation of two completely independent data sets by totally different models and obtaining a similar result. Nonetheless it is important to know how well the different lines in Figures 6–9 are constrained given uncertainties in the data used to generate them. We do this by solving three simultaneous equations of the type in equation (8). The first test, which is not tabulated here, was to determine three unknowns: the time rate of change of surface temperature, dT/dt, and the mass transfer coefficients for small and large bubbles, k_c and k_p, respectively (equations (A20) and (A21)) using input data for ΔN_2/Ar, ΔNe, and either ΔAr, or ΔNe/Kr presented in Table 2 and the model of *Liang et al*. [2013, hereinafter L13]. The dT/dt values derived for these unknowns were between −0.02 and −0.04 (°C/d^{-1}), which is consistent with the reanalysis result (Table 1). Mass transfer coefficients determined by this exercise were within ± 30% of those suggested by the L13 model. This result established the acceptability of the simultaneous equation approach to the error analysis.

The sensitivity of the noble gas concentrations and their ratios to the main environmental uncertainties was determined using a Monte Carlo error analysis for input values of the mixed layer depth (h = 175 ± 50), wind speed (U_{10} = 12.3 ± 1.2 m s^{-1}) and surface water cooling (dT/dt = 0.03 ± 0.01°C d^{-1}). Five hundred solutions for these input values varying randomly and independently about their means yielded uncertainties to the argon supersaturation of about ± 0.5% for each input value individually resulting in a total uncertainty for ΔAr of ± 1.0% (Table 3). The total error for the gas ratio ΔN_2/Ar is ± 0.2%, which suggests that this data is most effective in constraining the importance of the different bubble models. If we assume that the Monte Carlo error for each of the gas exchange models is similar to those calculated in Table 3 the uncertainty of the lines in Figures 6–9 is given in Table 3 and in the figure captions. The N_2/Ar data (Figure 6) clearly distinguish the different gas exchange models; however, it is not possible to say whether L13 or W97 is preferred because of uncertainty in the wind speeds and the model results. An uncertainty of ± 0.6% for ΔNe lines (Figure 7) indicate that the data are in accord with prediction of the L13 model. An error of ± 1.0% for the lines in Figure 8 still rules out the model of W09 but the uncertainty is too large to distinguish among the others. A ΔKr/Ar uncertainty of ± 0.6% is not large enough to explain the mismatch between the data and model noted previously.

4. Conclusions

Comparison of noble gas and N_2 measurements in the thermocline and surface ocean using two separate upper-ocean models indicate that bubble processes are an important mechanism controlling the saturation state of inert atmospheric gases, particularly in winter when wind speeds are high. Comparison of four different bubble models chosen to represent the breadth of current mechanistic model approaches indicates that formulations originating from the theoretical interpretation of bubble plumes do the best job of reproducing the measurements. Models of *Woolf* [1997] and *Liang et al*. [2013] come closest to explaining the data, but still overpredict the supersaturation of N_2 in late winter-early spring in the NE Pacific. The model of *Liang et al*. [2013] is presently preferred because it derives from a highly resolved bubble model, can be

applied to all insoluble gases, and it includes mechanisms for both bubbles that completely collapse, and those that are large enough to be submerged and reemerge to the atmosphere. Both of these mechanisms are important for interpreting observations of gases with a wide variety of solubilities. Improvement of present models so that they more accurately predict observed supersaturations of nonreactive gases will help interpret in situ measurements of oxygen supersaturation on unmanned platforms in terms of net community biological production.

Appendix A

Models used to describe the role of bubbles in the air-sea exchange of gases have evolved over the past 30 years from two separate origins: (1) physical models of bubble plume distributions and their effects on air-sea exchange [*Merlivat and Memery*, 1983; *Woolf and Thorpe*, 1991; *Vagle et al*., 2010; *Liang et al*., 2013] and (2) empirical models of noble gas (originally He) supersaturation so that the air-sea exchange of bomb-produced ^{3}He could be calculated [*Fuchs et al*., 1987; *Jenkins*, 1988; *Stanley et al*., 2009]. Wind-speed-dependent mass transfer coefficients derived from ocean tracer distributions [*Wanninkhof*, 2014; *Nightingale et al*., 2000, and references therein] have no explicit bubble mechanism even though bubbles probably affect the exchange process at high wind speeds. (See text Introduction.) In this Appendix A, we describe four different models of air-sea gas exchange that are used to derive the results in Figures 6–9. Definitions of the symbols and their units are listed in Table A1. Square brackets, [], indicate concentrations.

The diffusive exchange at the air-sea interface is described in all the models as a mass transfer coefficient, k_s (m s^{-1}), times the concentration difference between the mixed layer of the ocean, [C] (mol m^{-3}) and the concentration at saturation equilibrium with the atmosphere gas partial pressure, [C^s].

$$F_s = -k_s([C^s]) - [C]) \ \left(\text{mol m}^{-2}\,\text{s}^{-1}\right) \tag{A1}$$

Table A1. The Meaning of Symbols Used in Text Equations and Their Units

$[C]$	mol m^{-3}	Concentration of gas C
$[C^s]$	mol m^{-3}	Concentration of gas, C, at Henry's Law equilibrium with the atmospheric pC
C_d	unitless	Drag coefficient at the air-water interface
D^C	cm^2 s^{-1}	Molecular diffusion coefficient of gas, C
D_0	cm^2 s^{-1}	term used to make unites balance ($D_0 = 1.0$)
Δ_e	unitless	The fraction of supersaturation due to the "Equilibrium" supersaturation caused by bubble fluxes in the WT91 model
F_s	mol m^{-2} s^{-1}	Air-sea flux across the surface air-sea interface
F_b	mol m^{-2} s^{-1}	Air sea flux due to bubbles
F_p	mol m^{-2} s^{-1}	Air sea flux due to large bubbles that do not collapse
F_c	mol m^{-2} s^{-1}	Air-sea flux due to small bubbles that due collapse
G	m s^{-2}	Acceleration due to gravity
K_H	mol m^{-3} atm^{-1}	Henry's Law coefficient
k_s	m s^{-1}	Mass transfer coefficient for surface air-sea transfer
k_T	m s^{-1}	Mass transfer coefficient for both surface air-sea interface and bubbles (unique to the WT91 model)
k_b	m s^{-1}	Mass transfer coefficient for all bubbles
k_p	m s^{-1}	Mass transfer coefficient for exchange across large bubble interface
k_c	mol m^{-2} s^{-1}	Flux of air due to collapsing bubbles
P_a	Pascals	Atmospheric pressure
p_{H2O}	Pascals	Equilibrium water vapor pressure
ΔP	unitless	The fraction of supersaturation inside large bubbles that do not collapse in the models of S09 and L13
R	m^{3}Pa mol^{-1}K^{-1}	The gas constant
S_c	unitless	Schmidt number, = (D/ν)$^{0.5}$, where ν is the kinematic viscosity
T	^{o}K	Absolute temperature
U_{10}	m s^{-1}	Wind speed at 10 m height above the ocean
$U^*_{10,i}$	m s^{-1}	Threshold wind speed at which equilibrium saturation equal 1% (WT91 model)
u^a_*	m s^{-1}	Friction velocity on the air side of the air-water interface
u^w_*	m s^{-1}	Friction velocity on the water side of the air-water interface
X^c	unitless	Mole fraction of gas C in a dry atmosphere
z_b	m	Depth of large bubble penetration
B	unitless	Bunson solubility coefficient
β_x	unitless	Constant in the formula for k_b given in W97
ρ_a	kg m^{-3}	Atmospheric density
ρ_w	kg m^{-3}	Seawater density

A grand summary equation for the wind speed dependence of the gas exchange mass transfer coefficient is presented in *Wanninkhof et al*. [2009, hereinafter W09]:

$$k_s^* = \left(3 + 0.1(U_{10}) + 0.64(U_{10})^2 + 0.011(U_{10})^3\right)\left({}^{Sc}/_{660}\right)^{-0.5} \quad (\text{cm hr}^{-1}) \tag{A2}$$

$$k_s(ms^{-1}) = k_s^*(cm\ h^{-1})/(3600\ s\ h^{-1} \times 100\ cm\ m^{-1}) \quad (\text{m s}^{-1})$$

There are no explicit bubble terms in equation (A2), but it does have a cubic dependence on wind speed at in the highest range, which is the expected wind speed dependence for white caps. This expression is constrained by both the bomb-produced distribution of carbon-14 in the ocean and by results from purposeful tracer release experiments. *Wanninkhof et al*. [2009] and *Wanninkhof* [2014] demonstrate that this expression is only slightly different from the quadratic equations that preceded it.

Woolf and Thorpe [1991] determined the role of bubbles in air-sea gas exchange using a bubble plume model and suggested a simple expression in which a single parameter, Δ_e (unitless), represents the enhancement of surface gas saturation caused by bubble processes.

$$F_T = -k_T([C^s](1+\Delta_e) - [C]) \quad (\text{mol m}^{-2}\,\text{s}^{-1}) \tag{A3}$$

At $\Delta_e = 0$, when bubble processes are unimportant, this equation is equal in form to equation (A1). The mass transfer coefficient, k_T, in this model was determined by the two linear regions in the lower wind speed range of the gas exchange expression of *Liss and Merlivat* [1986] because it was assumed that bubble processes are unimportant in this range. Wolf and Thorpe assumed that the second linear region of the *Liss and Merlivat* expression continued at higher wind speeds. In the presence of bubbles, $(1+\Delta_e)$ is the fractional supersaturation caused by bubble processes at steady state when there is no net gas flux across the air-water interface. In this condition the flux of gas into the ocean by bubble processes exactly balances the flux out of the ocean by surface exchange across the air-sea interface. The value of the bubble induced supersaturation in their model was related to wind speed by:

$$\Delta_e = 0.01\left({}^{U_{10}}/_{U^*_{10,i}}\right)^2 \tag{A4}$$

where $U_{10,i}$ is the ten meter wind speed at which the value of Δ_e is 1%. In their model $U_{10,N2} = 7.2$ m s^{-1}, $U_{10,O2} = 9.6$ m s^{-1} and $U_{10,CO2} = 49$ m s^{-1}.

This expression was later modified by *Wolf* [1997] to consist of two mass transfer coefficients: one for the surface air-sea exchange, k_s, and the other caused by bubbles, k_b:

$$F_T = -(k_s + k_b)([C^s](1+\Delta_e) - [C]) \quad (\text{mol m}^{-1}\,\text{s}^{-1}) \tag{A5}$$

where k_s was defined from wind tunnel experiments [*Jahne et al*., 1987] and is a linear function of the air-side friction velocity, u_*^a:

$$k_s = 1.57x10^{-4}u_*^a\left({}^{Sc}/_{600}\right)^{-0.5} \quad (\text{m s}^{-1}) \tag{A6}$$

(Note that the units of k_s are given as cm hr^{-1} in *Woolf* [1997], but they are really m s^{-1} as indicated above.) The expression suggested for the bubble mass transfer coefficient was

$$k_b = 9.4x10^{-3}U_{10}^{3.41}\beta_x^{-1}\left[1 + \left(14\beta_x S_C^{-0.5}\right)^{-1/1.2}\right]^{-1.2} \quad (\text{cm hr}^{-1}) \tag{A7}$$

$$k_b(ms^{-1}) = k_s(cm\ h^{-1})/(3600\ s\ h^{-1} \times 100\ cm\ m^{-1}) \quad (\text{m s}^{-1})$$

The mass transfer coefficient determined by equation (A6) is very close to that in the first two wind speed regimens of *Liss and Merlivat* [1986, see Figure 1]. The relationship between u_*^a and the 10 meter wind speed is presented by *Large and Pond* [1981].

$$u_*^a = \sqrt{C_d}U_{10} \quad (\text{m s}^{-1}) \tag{A8}$$

$$C_d = 0.0012 \quad (U_{10} < 11\ ms^{-1}) \tag{A9}$$

$$= (0.49 + 0.065U_{10}) \times 10^{-3} \quad (U_{10} = 11 - 20\ ms^{-1})$$

$$= 0.0018 \quad (U_{10} > 20\ ms^{-1})$$

Equations (A4)–(A9) comprise the gas exchange expressions of *Woolf* [1997, hereinafter W97].

Air-sea gas exchange expressions that derived originally from attempts to understand noble gas supersaturation [*Fuchs et al*., 1987] categorized bubble fluxes into two main types: the flux from small bubbles that totally collapse when they are forced below the air-sea interface, F_c, and that from larger bubble that submerge, exchange gases and resurface, F_p. In these models the total flux is the sum of the surface air-water flux, F_s, and the bubble flux, F_b:

$$F_T = F_s + F_b \quad (\text{mol m}^{-2}\text{s}^{-1}) \tag{A10}$$

where

$$F_b = F_c + F_p \tag{A11}$$

Fluxes from the two different bubble types are controlled by very different mechanisms. Collapsing bubble fluxes are a function of a mass transfer coefficient, k_c, and the atmospheric mole fraction, X, only:

$$F_c = -k_c X^C \quad (\text{mol m}^{-2}\text{s}^{-1}) \tag{A12}$$

Larger bubbles that exchange gases across the bubble-water interface follow a mechanism analogous to that described by *Woolf and Thorpe* [1991] for the total gas exchange flux (A3):

$$F_p = -k_p((1 + \Delta P)[C^s] - [C]) \quad (\text{mol m}^{-2}\text{s}^{-1}) \tag{A13}$$

where ΔP in this model is the fractional increase in pressure experienced by the large bubbles.

In the model of *Stanley et al* [2009, hereinafter S09], ΔP, is calculated as the hydrostatic pressure inside large bubbles that are forced below the air-sea interface:

$$\Delta P = \frac{\rho_w g z_b}{RT}\left(\frac{\beta X^c}{[C^s]}\right) \tag{A14}$$

where the mean depth of large bubbles is a function of wind speed:

$$z_b = (0.15U_{10} - 0.55) \quad (\text{m}) \tag{A15}$$

Stanley et al. [2009] use the distribution of noble gases at the Bermuda Atlantic Time Series (BATS) to determine the mass transfer coefficients k_s, k_c, and k_p as:

$$k_s = 8.67x10^{-7}\ U_{10}^2 \left({}^{S_c}/_{660}\right)^{-0.5} \quad (\text{m s}^{-1}) \tag{A16}$$

$$k_c = 9.1x10^{-11}\ \frac{(P_a - P_{H_2O})X^c}{RT}(U_{10} - 2.27)^3 \quad (\text{mol m}^{-2}\text{s}^{-1}) \tag{A17}$$

$$k_p = 2.3x10^{-3}\left({}^{D^C}/_{D_0}\right)^{0.67}(U_{10} - 2.27)^3 \quad (\text{m s}^{-1}) \tag{A18}$$

The value of k_s determined in this model was similar to that proposed by the equations described in *Wanninkhof et al*., [2009, see Figure 1]. Equations (A1) and (A10) through (A18) describe the air sea flux in the model of *Stanley et al*., [2009, hereinafter S09].

The model of *Liang et al*. [2013, hereinafter L13], like that of *Woolf* [1997], was derived from a three-dimensional model of bubble plumes and is formulated using the same terms as the *Stanley et al*. [2009]

model; however, the mass transfer coefficients were determined differently. The value for k_s in the L13 model was taken to be that suggested by the NOAA-COAREG gas exchange model [*Fairall et al*., 2011], which is assumed to involve only the mechanism of surface air-sea exchange and is linear with respect to friction velocity.

$$k_s = 1.04x10^{-4} A\ u_*^a \left({}^{Sc}/_{660}\right)^{-0.5}\ \left(\text{m s}^{-1}\right) \tag{A19}$$

where A is evaluated to be 1.3 [*Jeffery et al*., 2010]. This relationship is very similar to the second linear range of mass transfer coefficient-wind speed relationship of *Liss and Merlivat* [1986] and the wind-tunnel value of *Jahne et al*. [1987] (see Figure 1).

Wind speed dependencies of the two bubble coefficients, k_c and k_p and the bubble produced increment of supersaturation, ΔP, were determined by *Liang et al*. [2013] from the model solution of the bubble distribution and gas transfer equations.

$$k_c = 5.56\left(u_*^w\right)^{3.86}\ \left(\text{mol m}^{-2}\text{s}^{-1}\right) \tag{A20}$$

$$k_p = 5.5\left(u_*^w\right)^{2.76}\left({}^{Sc}/_{660}\right)^{-0.67}\ \left(\text{m s}^{-1}\right) \tag{A21}$$

$$\Delta P = 1.52\left(u_*^w\right)^{1.06} \tag{A22}$$

where the water-side, u_*^w, and air-side, u_*^a, friction velocities are related by:

$$u_*^w = \left({}^{\rho_a}/_{\rho_w}\right)^{0.5} u_*^a = 0.034\sqrt{C_d}U_{10}\ \left(\text{m s}^{-1}\right) \tag{A23}$$

The equations describing the model of *Liang et al*. [2013, hereinafter L13] are (A10)–(A13) and (A19)–(A23).

Equations describing the bubble models of W97, S09, and L13 share similarities that are not immediately obvious. Combining equations (A1), (A10), and (A11–A13) and using the Henry's Law coefficient, K_H (mol m^{-3} atm^{-1}), with the approximation that the atmospheric gas partial pressure, pC, is equal to the mole fraction, X, $[C^s] = pC\ K_H \sim X\ K_H$, yields:

$$FT = -\left(k_s + k_p\right)\left\{\left[1 + \left(k_c/K_H + k_p\Delta P\right)/\left(k_s + k_p\right)\right] \times [C_s] - [C]\right\}\quad \left(\text{mol m}^{-2}\ \text{s}^{-1}\right) \tag{A24}$$

This equation is in the form of that proposed by *Woolf* [1997] (equation (A5)). If one equates the mass transfer coefficient for large bubbles in the S09 and L13 models, k_p, with the mass transfer coefficient of *Woolf* [1997] used for all bubbles, k_b, then the steady state supersaturation is equal to a combination of the mass transfer coefficients and the term for excess supersaturation in the surface waters caused by both small and large bubbles is:

$$\Delta_e = \left(k_c/K_H + k_p\Delta P\right)/\left(k_s + k_p\right) \tag{A25}$$

Substituting values for k_c, k_p, k_s and ΔP determined by the L13 model into equation (A25) results in a wind-speed dependence for Δ_e shown in Table A2. Values suggested by W97 are not greatly different for those predicted by the L13 model. Increasing the value for $U_{10,N2}$ in equation (A4) to 14 instead of 7.2, as suggested by *Vagle et al*. [2010] decreases the supersaturation value derived by the W97 model to values below those of L13.

Table A2. Comparison of Total Bubble-Induced Supersaturation, Δ_e, for N_2 at 20°C and S = 35 Calculated From Separate Sources[a]

U_{10} (m s^{-1})	C_d A9	u_*^a A8 (m s^{-1})	u_*^w A23 (m s^{-1})	k_p A21 (x10^5) (m s^{-1})	k_c A20 (x10^5) (mol/m^2 s)	k_s A16 (x10^5) (m s^{-1})	Δ_p A22	Δ_e A25 (L13)	Δ_e A4 (WT91)
2	0.0012	0.07	0.002	0.03		0.96	0.002	0.0002	0.0007
6	0.0012	0.21	0.007	0.65	0.003	2.8	0.008	0.003	0.007
10	0.0012	0.35	0.012	2.7	0.02	4.8	0.01	0.01	0.02
14	0.0015	0.52	0.018	8.3	0.10	7.3	0.02	0.02	0.04
20	0.0018	0.85	0.029	31.3	0.64	11.8	0.04	0.05	0.08

[a]The value in the last column is from *Woolf and Thorpe* [1991]. The values next to this column are derived from equation (A25) with the terms on the right hand side determined from the model of Liang et al. [2013]. Appendix A equations used for each calculation are indicated under the symbol.

Acknowledgments
We acknowledge Roberta Hamme for curating tables of the noble gas and N_2/Ar ratio data on her web site (www.uvic.ca/~hamme/). We thank Bill Jenkins and Dempsey Lott for sharing preliminary, unpublished results for the solubility of Kr. Henry Bittig and two anonymous reviewers pointed out inconsistencies that have been repaired resulting in a better paper. The surface ocean N_2 data from Ocean Station Papa are unpublished and available from the first author. Parts of this research began as a problem in a graduate-level chemical tracers class at University of Washington. S. E. would like to thank the students for being involved in the initial phase of the arguments presented here. This research was funded by NSF grants Oce1154001 and Oce 1458888.

References

Bushinsky, S., and S. Emerson (2015), Marine biological production from remote in situ oxygen measurements on a profiling float in the subarctic Pacific Ocean, *Global Biogoechem. Cycles*, *29*, 2050–2060, doi:10.1002/2015GB005251.

Chang, B. X., A. H. Devol, and S. Emerson (2010), Denitrification and the nitrogen gas excess in the eastern tropical South Pacific oxygen deficient zone, *Deep Sea Res., Part I*, *57*, 1092–1101.

Cronin, M. F., N. Pelland, S. Emerson, and W. R. Crawford (2015), Estimating diffusivity from the missed layer heat and salt balances in the North Pacific, *J. Geophys. Res. Oceans*, *120*, 7346–7362, doi:10.1002/2015JC011010.

Emerson, S. (2014), Annual net community production and biological carbon flux in the ocean, *Global Biogeochem. Cycles*, *28*, 14–28, doi:10.1002/2013GB004680.

Emerson, S., C. Stump, and D. Nicholson (2008), Net biological oxygen production in the ocean: Remote in situ measurements of O_2 and N_2 in surface waters, *Global Biogeochem. Cycles*, *22*, GB3023, doi:10.1029/2007GB003095.

Emerson, S., T. Ito, and R. H. Hamme (2012), Argon supersaturation indicates low decadal-scale mixing in the subtropical thermocline, *Geophys. Res. Lett.*, *39*, L18610, doi:10.1029/2012GL053054.

Fairall, C. W., E. F. Bradley, J. E. Hare, A. A. Grachev, J. B. Edson (2003), Bulk parameterization of air-sea fluxes: Updates and verification for the COARE algorithm, *J. Clim.*, *16*, 571–591.

Fairall, C. W., M. Yang, L. Bariteau, J. B. Edson, D. Helmig, W. McGillis, S. Pezoa, J. E. Hare, B. Huebert, and B. Blomquist (2011), Implementation of the coupled ocean-atmosphere response experiment flux algorithm with CO_2, dimethyl sulfide, and O_3, *J. Geophys. Res.*, *116*, C00F09, doi:10.1029/2010JC006884.

Fuchs, G., W. Roether, and P. Schlosser (1987), Excess ^{3}He in the ocean surface layer, *J. Geophys. Res.*, *92*, 6559–6568.

Goddijn-Murphy. L., D. L. Woolf, A. H. Callaghan, P. D. Nightingale, and J. D. Shutter (2016), A reconciliation of empirical and mechanistic models of the air-sea transfer velocity, *J. Geophys. Res. Oceans*, *121*, doi:10.1002/2015JD011096, in press.

Gruber, N., and J. L. Sarmiento (1997), Global patterns of marine nitrogen fixation and denitrification, *Global Biogeochem. Cycles*, *11*, 235–266, doi:10.1029/97GB00077.

Hamme, R. C., and S. R. Emerson (2004), The solubility of neon, nitrogen, and argon in distilled water and seawater, *Deep Sea Res., Part I*, *51*, 1517–1528.

Hamme, R. C., and S. R. Emerson (2006), Constraining bubble dynamics and mixing with dissolved gases: Implications for productivity measurements and oxygen mass balance, *J. Mar. Res.*, *64*, 73–95.

Hamme, R. C., and S. R. Emerson (2013), Deep-sea nutrient loss inferred from the dissolved N_2/A ratio, *Geophys. Res. Lett.*, *40*, 1-5, doi:10.1002/grl.50275.

Hamme, R. C., and J. P. Severinghaus (2007), Trace gas disequilibria during deep-water formation, *Deep Sea Res., Part I*, *54*, 939–950.

Hare, J. E., C. W. Fairall, W. R. McGillis, J. B. Edson, B. Ward, and R. Wanninkhof (2004), Evaluation of the National Oceanic and Atmospheric Administration/Coupled-Ocean Atmospheric Response Experiment (NOAA/COARE) air-sea gas transfer parameterization using GasEx data, *J. Geophys. Res.*, *109*, C08S11, doi:10.1029/2003JC001831.

Ho, D. T., R. Wanninkhof, P. Schlosser, D. S. Ullman, D. Herbert, D. S. Sullivan (2011), Toward a universal relationship between wind speed and gas exchange: Gas transfer velocities measured with ^{3}He/SF_6 during the Southern Ocean Gas Exchange Experiment, *J. Geophys. Res.*, *116*, C00F04, doi:10.1029/2010JC006854.

Ito, T. and C. Deutsch (2006), Understanding the saturation state of argon in the thermocline: The role of air-sea gas exchange and diapycnal mixing, *Global Biogeochem. Cycles*, *20*, GB3019, doi:10.1029/2005GB002655.

Jahne, B., K. O. Munnich, R. Bosinger, A. Dutzi, W. Huber, and P. Libner (1987), On the parameters influencing air-water gas exchange, *J. Geophys. Res.*, *92*, 1937–1949.

Jeffery, C. D., I. S. Robinson, and D. K. Woolf (2010), Tuning a physically-based model of the air-sea gas transfer velocity, *Ocean Modell.*, *31*, 28–35, doi:10.1016/j.ocemod.2009.09.001.

Jenkins, W. J. (1988), The use of anthropogenic tritium and helium-3 to study subtropical gyre ventilation and circulation, Philos. *Trans. R. Soc. London A*, *325*, 43–61.

Kanwisher, J. (1963), Effect of wind on CO_2 exchange across the sea surface, *J. Geophys. Res.*, *68*, 3921–3927.

Keeling, R. F. (1993), On the role of large bubbles in air-sea gas exchange and supersaturation in the ocean, *J. Mar. Res.*, *51*, 237–271.

Large, W. P., and S. Pond (1981), Open ocean momentum flux measurements in moderate to strong winds, *J. Phys. Oceanogr.*, *11*, 324–336.

Liang, J.-H., C. Deutsch, J. C. McWilliams, B. Baschek, P. P. Sullivan, and D. Chiba (2013), Parameterizing bubble-mediated air-sea gas exchange and its effect on ocean ventilation, *Global Biogoechem. Cycles*, *27*, 894–905, doi:10.1002/gbc.20080.

Liss, P. S., and L. Merlivat (1986), Air-sea gas exchange rates: Introduction and synthesis, in *The Role of Air-Sea Exchange in Geochemical Cycling*, edited by P. Buat-Menard and D. Reidel, pp. 113–127, Dordrect, Netherlands.

McNeil, C. L., B. Johnson, and D. M. Farmer (1995), In-situ measurement of dissolved nitrogen and oxygen in the ocean, *Deep Sea Res., Part I*, *42*, 819–826, doi:10.1016/0967-0637(95)97829.

Merlivat, L., and L. Memery (1983), Gas Exchange across an air-water interface: Experimental results and modeling of bubble contribution to transfer, *J. Geophys. Res.*, *88*, 707–724.

Nicholson, D., S. Emerson, S. Khatiwala, R. C. Hamme (2011), An inverse approach to estimate bubble-mediated air-sea gas flux from inert gas measurements, in *Proceedings on the 6th International Symposium on Gas Transfer at Water Surfaces*, edited by S. Komori, and R. Karose, pp. 223–237, Kyoto Univ. Press, Kyoto, Japan.

Nightingale, P. D., G. Malin, C. S. Law, A. J. Watson, P. S. Liss, M. I. Liddicoat, J. Boutin, and R. C. Upsill-Goddard (2000), In situ evaluation of air-sea gas exchange parameterizations using novel conservative and volatile tracers, *Global Biogeochem. Cycles*, *14*, 373–387.

Spitzer, W., and W. Jenkins (1989), Rates of vertical mixing, gas exchange and new production: Estimates from seasonal gas cycles in the upper ocean near Bermuda, *J. Mar. Res.*, *47*, 69–196.

Stanley, R., W. Jenkins, D. Lott, and S. Doney (2009), Noble gas constraints on air-sea gas exchange and bubble fluxes, *J. Geophys. Res.*, *114*, C11020, doi:10.1029/2009JC005396.

Steiner, N., S. Vagle, K. Denman, and C. L. McNeil (2007), Oxygen and nitrogen cycling in the North-East Pacific-–Simulations and observations at Station Papa in 2003/2004, *J. Mar. Res.*, *65*(3), 441–469.

Suga, T., K. Motoki, Y. Aoki, and A. M. Macdonald (2004), The North Pacific climatology of winter mixed layer and mode waters, *J. Phys. Oceanogr.*, *34*, 3–34.

Vagle, S., C. McNeil, and N. Steiner (2010), Upper ocean bubble measurements from the NE Pacific and estimates of their role in air-sea gas transfer of the weakly soluble gases nitrogen and oxygen, *J. Geophys. Res.*, *115*, C12054, doi:10.1029/2009JC005990.

Wanninkhof, R. (1992), Relationship between wind speed and gas exchange over the ocean, *J. Geophys. Res.*, *97*, 7373–7382.
Wanninkhof, R. (2014), Relationship between wind speed and gas exchange over the ocean revisited, *Limnol. Oceanogr. Methods*, *12*, 351–362.
Wanninkhof, R., W. E. Asher, D. T. Ho, C. Sweeney, and W. R. McGillis (2009), Advances in quantifying air-Sea gas exchange and environmental forcing, *Annu. Rev. Sci.*, *1*, 213–244, doi:10.1146/annurev.marine.010908.163742.
Weiss R. F., and K. Kyser (1978), Solubility of krypton in water and seawater, *J. Chem. Thermodyn.*, *23*, 69–72.
Woolf, D. K. (1997), Bubbles and their role in gas exchange, in *The Sea Surface and Global Change*, edited by P. S. Liss and R. A. Duce, pp. 173–206, Cambridge Univ. Press, N. Y., doi:10.1017/CBO9780511525025.007.
Woolf, D. K., and S. Thorpe (1991), Bubbles and the air-sea exchange of gases in near saturation conditions, *J. Mar. Res.*, *49*, 435–466, doi: 10.1357/002224091784995765.